# Decay of deformed $^{59}$Cu nuclei

G. Viesti,[a]* B. Fornal,[b]† D. Fabris,[c] K. Hagel,[c] J. B. Natowitz,[c] G. Nebbia,[a] G. Prete,[b] and F. Trotti[a]
[a]*Istituto Nazionale di Fisica Nucleare and Dipartimento di Fisica dell'Università di Padova, I-35131 Padova, Italy*
[b]*Istituto Nazionale di Fisica Nucleare, Laboratori Nazionali di Legnaro, I-35020 Legnaro (Padova), Italy*
[c]*Cyclotron Institute, Texas A&M University, College Station, Texas 77843*
(Received 19 April 1988)

The light charged particle emission following the fusion of $^{32}$S with $^{27}$Al at 100–150 MeV bombarding energies in 10 MeV steps has been studied. Energy spectra and angular distributions of $p$, $d$, $t$, and alpha particles as well as light-particle–light-particle coincidences have been measured. The light charged particle data and the published evaporation residue distributions are compared with statistical model calculations. The comparison shows that the statistical model describes well the experimental observables if account is taken of changes in the level density and barrier apparently due to the onset of deformations at high spins. The spectra of $\alpha$ particles emitted from narrow windows of angular momentum with $28\hbar \leq J_{\text{ave}} \leq 34\hbar$ have been obtained by means of a subtraction procedure and analyzed to extract emission barriers and level density enhancement factors. The deduced barrier lowering with respect to the spherical barrier is somewhat greater than that predicted by assuming rotating liquid drop model (RLDM) shapes. The level density enhancement factor is comparable with that determined in the past for statistically deformed nuclei.

## I. INTRODUCTION

Compound nucleus formation and decay has been studied for a long time both from the theoretical and the experimental point of view. Statistical theories describe the decay of the fully equilibrated compound nucleus and the competition among the open decay channels. Model calculations based on statistical theories are today a common and powerful tool to evaluate cross sections and branching ratios for light-particle induced nuclear reactions.[1]

With heavy-ion beams, compound nuclei may be produced with high excitation energies and angular momenta far from those populated using light projectiles;[2] at high excitation energy, the meltdown of the nuclear structure is predicted.[3] High excitation energy implies that the nucleus deexcites by emitting several particles and gamma rays so that the decay pattern involves a number of different paths.

High spins are expected to favor the emission of complex clusters which are more effective than nucleons in removing the angular momentum. This effect contributes to further complicate the decay cascade.[4] The population of high spin states may induce angular momentum driven dynamical deformations of the hot nucleus[5] which will introduce additional deviations from low-energy light-ion-induced reactions.

Statistical theory appears, in general, to fit the data of heavy-ion induced reactions when the basic formalism of the model is applied at each decay step and summed over all the decay products.[2] The basic formalism normally includes the relevant structure information available for nuclei near stability in the form of optical model (OM) transmission coefficients and of level densities based on light-particle-induced reaction studies. Models like the rotating liquid drop model (RLDM) are used to predict the spin dependence of the deformation and the Fermi-gas model (FGM) is used to evaluate the level density at high excitation energy.

Several questions have been raised about the use of ingredients, derived for cold nuclei at low spin, for nuclei produced in heavy-ion-induced reactions, and efforts have been made to develop more refined calculations.[6] Despite the progress made in the field, the situation is today not completely clear; for example, the majority of the statistical model computer codes in use evaluate the yrast line from the RLDM, so that the nucleus is supposed to be dynamically deformed at high spin. The level density built on the RLDM yrast line is that of a spherical nucleus at low as well as at high angular momentum although differences in level density between spherical and deformed nuclei are well known in the case of statically deformed nuclei,[7,8] a similar contradiction appears in the case of transmission coefficients. Calculations of $T_l$ for deformed nuclei have been developed and the effect of this parameter on the evaporation calculation has been studied in detail.[9,10]

In this work we studied evaporation from the $^{59}$Cu compound nucleus populated by the $^{32}\text{S}+^{27}\text{Al}$ reaction at moderate excitation energies ($E^*=60-80$ MeV) and at spin values for which sizable deformations are predicted. This particular reaction was selected because previous work provided evidence for a strong influence of deformation on the particle spectra,[11] the present data include light particle ($p,d,t,\alpha$) energy spectra and angular distributions as well as light-particle–light-particle correlations. Those data, together with the published evaporation residue distributions,[12,13] are compared with detailed evaporation calculations.

One goal of this work was a global test of the statistical model calculations and of their basic ingredients such as level densities and transmission coefficients in this range

 

of masses, spins, and excitation energies. A second goal was to look for deformation effects. A brief report on this work was previously published.[14]

## II. EXPERIMENTAL METHODS

The experiments were performed at the XTU Tandem of the Laboratori Nazionali di Legnaro. The beam of $^{32}$S at incident energies from 100 MeV to 150 MeV in 10 MeV step was used to bombard the targets of 170 and 500 $\mu$g/cm$^2$ of $^{27}$Al. The corresponding excitation energies and spin regions populated in the compound nucleus $^{59}$Cu are shown in the Table I.

Light particles $p$, $d$, $t$, $^3$He, and $\alpha$ were detected with four three-member silicon telescopes ($\Delta E_1 = 17-32$ $\mu$m, $\Delta E_2 = 150-400$ $\mu$m, $E_{res} = 2000-5000$ $\mu$m) having aperture angles of 2°, initially placed at 30°, 60°, 120°, and 150° with respect to the beam. During the experiment the detectors were shifted in the horizontal plane by $\Delta\theta = +7.5°$ and $+15°$ and data were taken at the new angles.

The telescopes were calibrated relative to the 5.486 MeV $\alpha$ particle of $^{241}$Am. The stability of electronics and the dead time of the acquisition system were monitored during the measurements by precision pulsers. Relative normalizations of cross sections were obtained using an ionization chamber with an acceptance angle $\Delta\theta = 2.5°$ at $\theta_{lab} = 8°$ as a monitor.

In a second experiment the coincidences between light particles $\alpha$-$\alpha$, $p$-$\alpha$, and $p$-$p$ were observed with two $\Delta E$-$E$ telescopes ($\Delta E = 50$ $\mu$m, $E_{res} = 2000$ $\mu$m) placed at $\theta_{lab} = \pm 60°$ in the horizontal plane. They were about 9 cm from the target and had $\Delta\theta = 4°$ aperture angles.

Absolute cross sections at all beam energies were derived in both experiments by calibrating the Faraday Cup using the Rutherford scattering from a gold target. Data were recorded event by event on magnetic tape and then analyzed to extract energy spectra of light particles $p$, $d$, $t$, $^3$He, and $\alpha$.

The possibility exists that the singles spectra might be contaminated by light particles emitted from projectile-like and target-like fragments. For the similar reaction $^{40}$Ar+$^{27}$Al this contamination has been experimentally determined to be $\sim 1\%$ at the bombarding energies of 190 MeV and less than 10% at 240 MeV.[16,17] In this experiment, the 150 MeV irradiation is quite close in its dynamical conditions to the 190 MeV $^{40}$Ar experiment and we expect the contamination be as low as in that case.

TABLE I. Fusion of $^{32}$S on $^{27}$Al studied in this work.

| $E_{beam}$ (MeV) | $E_{\frac{1}{2}\ target}$ (MeV) | $E^*$ (MeV) | $\sigma_{fus}$ (mbarn)[a] | $J_{max}$ ($\hbar$)[b] |
|---|---|---|---|---|
| 100 | 98.7 | 58.6 | 760 | 27 |
| 110 | 106.2 | 62.1 | 860 | 30 |
| 120 | 118.8 | 67.8 | 930 | 33 |
| 130 | 126.4 | 71.3 | 950 | 34 |
| 140 | 138.8 | 77.0 | 1030 | 38 |
| 150 | 146.6 | 80.6 | 1040 | 39 |

[a]From Ref. 15.
[b]Calculated from the fusion cross section.

## III. EVAPORATION CALCULATION

According to the independence hypothesis, the statistical deexcitation of a compound nucleus may be calculated using the Hauser-Feshbach formalism subject to conservation of mass, charge, energy, and angular momentum, in the case of heavy-ion-induced reactions, these kinds of calculations require extensive numerical operations. Only few computer codes have been developed to follow the step-by-step decay of highly excited and rotating compound nuclei,[2] the computer code CASCADE (Ref. 18) and its Monte Carlo version CACARIZO,[11] which incorporates semiclassical angular distributions to describe the light particle emission, have been used extensively in this work, the CASCADE calculation derives the initial spin distribution of the compound nucleus from the known fusion cross section using a strong-absorption model and then calculates relative decay widths for $n$, $p$, $\alpha$, and $\gamma$-ray emission.

The particle emission probability $P_J(\nu,\epsilon)$ for the evaporation of the particle $\nu$ with energy $\epsilon$ and angular momentum $l$ from the compound nucleus with the angular momentum $J$ is expressed as the product of the transmission coefficient $T_l^{\nu}(\epsilon)$ and the level density $\rho_f(E_f,J_f)$ in the daughter nucleus. The population of the open channels is followed in the calculation by applying iteratively the Hauser-Feshbach formalism until the excitation energy is dissipated by emitted particles and $\gamma$ rays.

The transmission coefficients $T_l^{\nu}(\epsilon)$ needed at any decay step are extracted from the inverse process, i.e., the reaction between the incoming particle $\nu$ and the daughter nucleus by means of the optical model. However, these reactions have been investigated experimentally only for target nuclei in their ground states and all parameters of the OM potentials are for cold nuclei at low spin.

It is expected that the deformation of the compound nucleus such as predicted by the RLDM, modifies the evaporation barrier (and therefore the $T_l$). Classical sharp cutoff transmission coefficients have been calculated for deformed nuclei by numerical integration of $T_l$ over the surface of the spheroid predicted by the RLDM.[9] As discussed in Refs. 9 and 12 $T_l$ may also be modified by increasing the optical potential radius. This way of lowering the emission barrier has been applied in studies of $^{40}$Ar+$^{27}$Al and $^{32}$S+$^{27}$Al reactions.[11,17]

The second crucial quantity for the statistical model calculations is the nuclear level density. At low excitation energy the level density is usually determined from the angular momentum dependent level density formula for a spherical nucleus given by Lang[19] with the parametrization of $a$ and $\Delta$ from Dilg *et al.*[20] At high excitation energy the code CASCADE uses the Lang formula with parameters from the liquid drop model.

The level density formula implies an yrast line defined by the condition

$$E_{yr}=J(J+1)\hbar^2/2\mathcal{T}+\Delta \ .$$

The deformability under rotation is taken into account by assuming

$$\mathcal{T}=\mathcal{T}_{sphere}(1+DEF\times J^2+DEFS\times J^4) \ .$$

Because of the connection between the yrast line and the level density one may change the latter by changing the deformability parameters *DEF* and *DEFS*. This in turn implies a change in calculated relative decay probabilities, and in the shape of light particle spectra.

In this work CASCADE and CACARIZO calculations have been performed with the two sets of input parameters listed in Table II. The first is the set used by Puhlhofer *et al.*[12] to calculate the evaporation residue distribution at 160 MeV in the reaction $^{32}S+^{27}Al$ (this set is very close to the default options contained in CASCADE). The second was obtained by Choudhury *et al.*[11] by fitting the alpha particle spectra observed in the 214 MeV reaction and contains empirically adjusted parameters.

It has been verified that several small differences in the input parameters (IFACT, AFACT, and $E_{HE}$ in Table II) produce only slight differences in the calculated quantities. The most crucial factors in the model calculations are the definition of the yrast line and the optical model radii.

Set 1 assumes the yrast line as given by the RLDM with a small deformability parameter, producing a line close to the recent predictions of Mustafa[25] and Sierk.[26] Set 2 uses larger values of DEF and DEFS and the corresponding yrast line lies below the Mustafa and Sierk predictions above $J>27\hbar$. Those two yrast lines are shown in Fig. 1.

As discussed in Ref. 17 it appears that the lowering of the yrast line, required to reproduce the light particle spectra, is an artificial way of increasing the level density at the higher spin values. This effect will be discussed in the next section.

Both data sets have been used with transmission coefficients calculated with a reduced emission barrier. The corresponding multiplicative factor for the potential radius was RFACT=1.10 in Ref. 12 and RFACT=1.5 in Ref. 11. In this work all calculations labeled "set 1" have been performed with RFACT=1.10, those labeled "set 2" have employed RFACT=1.0–1.3 depending on the bombarding energy. Here the RFACT value was chosen to reproduce the low-energy part of the evaporative spectra.

For sake of comparison, results from the PACE2 (Ref. 27) code are also shown in Sec. III A to verify the relative independence of the findings from the specific program.

### A. Proton and alpha particle singles

The energy spectra of the light particles emitted in the decay of an equilibrated compound nucleus have often been used to probe the nuclear structure of excited nuclei.

TABLE II. Parameters for the evaporation calculations using CASCADE and CACARIZO.

| |
|---|
| Angular momentum distribution in the compound nucleus |
| (1) $J_{max}$ derived from $\sigma_{fus}$ (Table I) |
| (2) Diffuseness $\Delta=3.5\hbar$ |
| Optical potential for emitted particles |
| (1) Neutrons, Wilmore, and Hodgson (Ref. 21) |
| (2) Protons, Perey (Ref. 22) |
| (3) $\alpha$ particles, Huizenga and Igo (Ref. 23) |
| (4) Radius parameter multiplication factor RFACT: set 1: RFACT=1.10; set 2: RFACT=1.00–1.25 |
| Level density parameters at low excitation ($E^*\leq 10$ MeV) |
| (1) Fermi-gas level density formula (Ref. 19) with empirical parameters from Dilg (Ref. 20) |
| (2) Effective moment of inertia $\mathcal{T}=$IFACT$\times\mathcal{T}_{rigid}$: set 1: IFACT=0.95; set 2: IFACT=1.00 |
| Level density parameters at high excitation ($E^*\geq E_{HE}$ MeV) set 1: $E_{HE}=15$ MeV; set 2: $E_{HE}=20$ MeV) |
| (1) Fermi-gas level density formula (Ref. 19) with parameters from liquid drop model (Ref. 24). |
| (2) Level density parameter $a_{LDM}=A/$AFACT MeV$^{-1}$: set 1: AFACT=8.5; set 2: AFACT=8.0 |
| Yrast line |
| (1) Moment of inertia for rigid body with radius parameter $r_0$: set 1: $r_0=1.28$; set 2: $r_0=1.30$ |
| (2) Deformability parameters used to calculate the effective moment of inertia $\mathcal{T}=\mathcal{T}_{sphere}\times(1+DEF\times J^2+DEFS\times J^4)$ as a function of the angular momentum $J$: |
| set 1: DEF=$10^{-4}$; set 2: DEF=$2.3\times10^{-4}$; |
| set 1: DEFS=0.0; set 2; DEFS=$0.16\times10^{-6}$ |

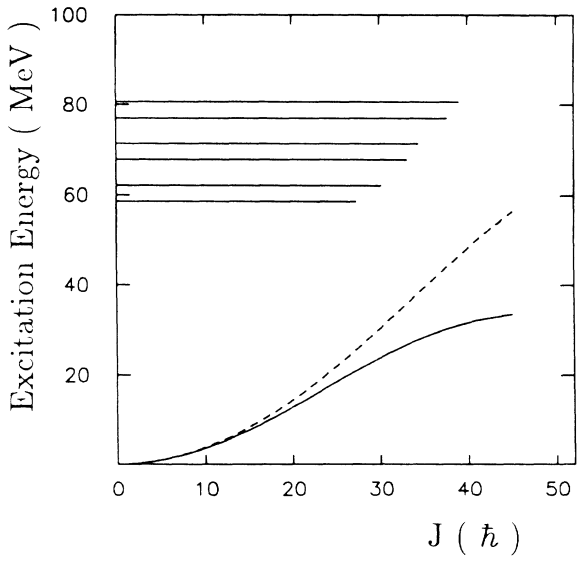


FIG. 1. Yrast plot for $^{59}$Cu. Yrast lines are shown following set 1 (dashed line) and set 2 (solid line) of input data for the statistical model calculation. The heavy horizontal lines indicate the angular momentum range and excitation energies associated with the fusion reaction studied in this work. For details see the text.

In the case of first step emission, the spectral shape carries unambiguous information on the emission barrier and the level density of the residual nucleus.[28] This information can be related to the shape of the emitter.

In heavy-ion reactions the deexcitation cascade generally involves several steps and comparison with model calculations and/or unfolding procedures are needed to derive from the experimental spectra those quantities related to the emitting system at the initial excitation energy and spin.

As evidenced in the work of Choudhury *et al.*,[11] the alpha particle spectra from the fusion of 100 MeV $^{32}$S+$^{27}$Al are quite well described by statistical model calculation considering the emitting nucleus to be nearly spherical. This kind of calculation fails to describe the spectra taken at 214 MeV bombarding energy which involve higher spins in the emitter and apparent strong deformation, as described by the RLDM.

This same effect is evident in Fig. 2(a) where $\alpha$ spectra taken at bombarding energies between 100 and 150 MeV are compared with the calculation using the parameters of set 1 which contains, as discussed above, the RLDM yrast line and transmission coefficients which fit the barrier region at 100 MeV bombarding energy. Increasing deviations between experimental and calculated spectra appear as the bombarding energy is raised. The same effect is not so apparent in the case of proton emission [Fig. 2(b)]. The agreement between the experimental and calculated proton spectra is fairly good and appears independent of the bombarding energy. The excess of energetic particles in the calculation is mainly due to first chance alphas emitted from the high spin states.

We verified that the failure in describing the $\alpha$ spectra at energies larger than 100 MeV was independent of the particular computer program used. Calculations were performed at all energies with the code PACE2 with default parameters which are close to the set 1 input data. In particular, the yrast line in the PACE2 calculation is very close to that obtained with our set 1 parameters. PACE2 uses transmission coefficients averaged over the deexcitation cascade. We have made no attempt to adjust that average to that which would result in the CASCADE calculation. We show in Fig. 3 a typical comparison between PACE2 and CASCADE.

As in the previous work,[11,17] an adjusted statistical model calculation (i.e., using the input set 2) is able to reproduce the experimental spectra. The input adjustments effective in changing the spectral shape are (1) an increase of the OM potential radii which results in a lowering of the average emission barriers, increasing the yield of low-energy $\alpha$ particles; (2) a spin dependent increase of the level density, obtained by lowering the yrast line which removes the excess of high-energy $\alpha$ particles.

In Figs. 4 and 5 we compare calculated laboratory spectra at selected angles for alphas and protons with the experimental spectra. The ratio of the deformed to spherical potential radius used in the calculations ranges from RFACT=1.00 at 100 MeV to RFACT=1.25 at 150 MeV, increasing linearly with the bombarding energy. The CACARIZO calculation with set 2 input, accounts well for the shapes of the $\alpha$ spectra. The calculated $p$ spectra (set 2 input) are in better agreement with the experimental data than the set 1 calculations, although the agreement is not as good as that observed for $\alpha$ spectra. Even lower barriers seem to be required. In Fig. 6 the measured angular distributions are compared with the calculated ones. We note that the angular distributions of Fig. 6 are for energetic particles, $E_\alpha \geq 17$ MeV and $E_p \geq 5$ MeV in the COM system, because of the experimental threshold for the backward angle measurements. The measured anisotropies increase with increasing bombarding energies from $\sim 2$ to $\sim 5$ for alpha and from $\sim 1.3$ to $\sim 2.3$ for protons. These anisotropies are to be compared with $W(160°)/W(90°) \sim 1.5$ for alpha and $W(160°)/W(90°) \sim 1.1$ for protons evaporated from Ni, Co, Cu compound nuclei in alpha induced reactions.[29] Anisotropies of $\sim 2.5$ for alpha and $\sim 1.5$ for protons have been measured in the case of the $^{40}$Ar+$^{27}$Al reaction at 190 MeV.[16] Only the set 2 calculations are reported in Fig. 6; set 1 gives very similar results.

The alpha particle angular distributions are reproduced reasonably well by the calculations. Deviations appear at the higher bombarding energies for angles larger than 160°. More dramatic is the difference between calculation and experiment in the proton case. The model calculations produces flat distributions with some small fluctuations (within 10%). This is not surprising because the semiclassical approximations are known to work well for values of the emitter spin $J$ and for the angular momentum $l$ carried away by the particle such that $J > l > 1$. The rather small sensitivity of the proton spectra to the spin dependence of the level density (i.e., to the lowering of the yrast line) demonstrates that those particles carry small angular momentum $l$. The deviations in

the angular distributions of Fig. 6 might suggest that the protons need a complete quantum-mechanical treatment.

Figure 7 shows the alpha-to-proton ratio at different detection angles. As is the case for the shapes of the alpha spectra, the difference between the two input sets appears clearly. Set 1 overestimates the alpha-to-proton ratio mainly because of the excess of first chance alpha particles. Set 2 is able to reproduce correctly both the spec-

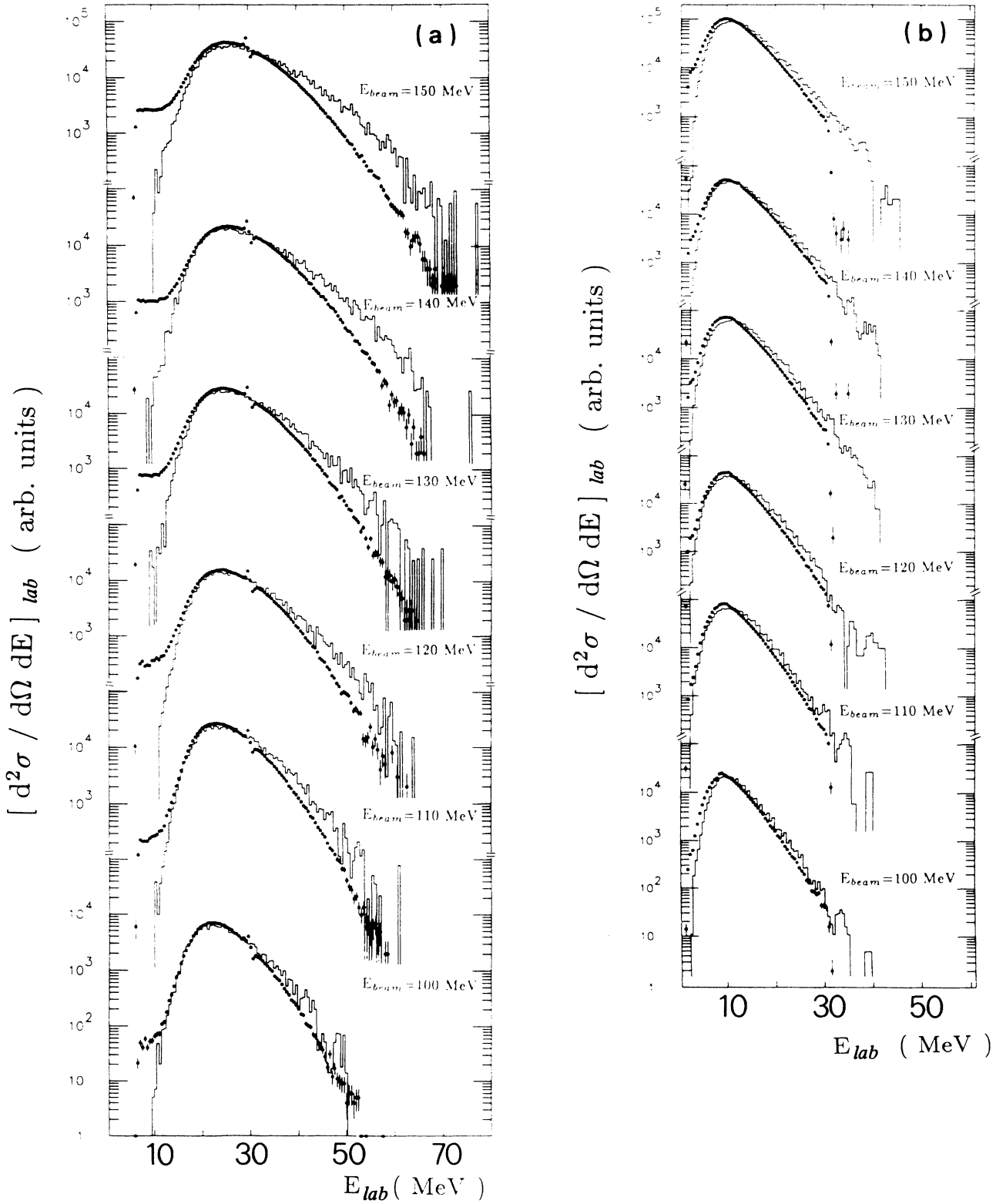


FIG. 2. Experimental and calculated alpha particle (a) and proton (b) spectra for 100–150 MeV bombarding energies at $\theta_{lab}=30°$. Calculations are standard statistical model (set 1) using the CACARIZO code.

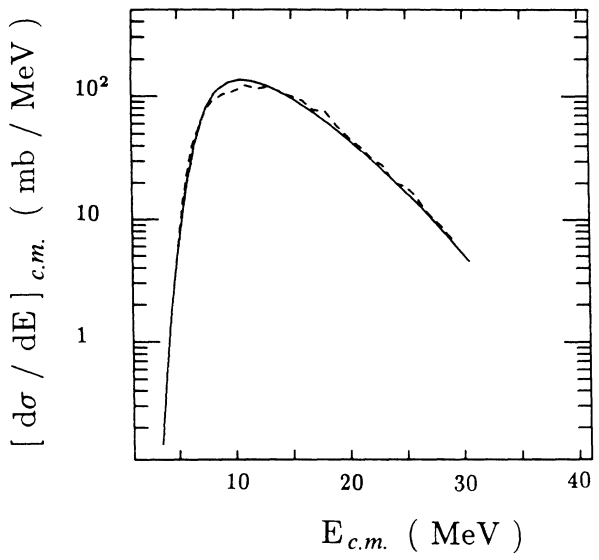


FIG. 3. Example of comparison between CASCADE (set 1) and PACE2. Calculated COM alpha particle spectra at 150 MeV bombarding energy.

tral shapes and relative cross sections of alpha and proton emission. The reduction of the $\alpha$ emission from the high spin states in the first decay step propagates in the cascade changing the average paths during the deexcitation. Looking in detail at the Monte Carlo simulation, we found that set 2 allows the emission of more nucleons in the cascade and that the average emission step for $\alpha$ particles occurs later in the cascade.

### B. Evaporation residue distribution

The CASCADE code has been successfully employed in the past to calculate evaporation residue (ER) distributions for compound nuclei with $A \leq 100$.[12,13,18,30,31]

In the work of Refs. 12 and 13, ER's distribution from the reaction $^{32}S+^{27}Al$ are well reproduced by the CASCADE code. These calculations employed set 1 input taking into account also the experimentally known levels of the residual nuclei to define the yrast line and the level densities at low excitation energy. The ER distribution $d\sigma_{ER}/dA$ was accounted for by the model calculation with an average deviation in cross section of $\sim 20\%$ at both 130 and 160 MeV bombarding energies. The same quality of fit is obtained using the input data of set 1 without inclusion of the experimental levels. The results of this model calculation are reported in Fig. 8.

A comparable reproduction of the experimental distribution is also obtained by using the input data set 2 using radius multiplication factors of 1.2 and 1.3 for the calculation at 130 and 160 MeV, respectively. The average deviation in cross section is in this case $\sim 25\%$.

While the calculated ER distribution is clearly sensitive to the input parameters, the global comparison between the experimental and calculated distributions does not allow a clear choice of parameters to be made.

TABLE III. Comparison between yields for light-particle–light-particle correlations (relative to singles) and statistical model calculations. For details see the text. $E_{beam}=150$ MeV; $\theta_1=\theta_2=60°$; $\Delta\phi=180°$. Reported values are $\times 10^{-2}$.

| Type of correlation | Experimental | Calculated set 1 | Calculated set 2 |
|---|---|---|---|
| $\alpha$-$\alpha_{coinc}/\alpha_{sing}$ | 1.7 | 1.9 | 1.6 |
| $\alpha$-$p_{coinc}/\alpha_{sing}$ | 2.8 | 1.6 | 2.2 |
| $p$-$\alpha_{coinc}/p_{sing}$ | 1.2 | 1.1 | 1.0 |
| $p$-$p_{coinc}/p_{sing}$ | 2.0 | 1.6 | 1.8 |

### C. Light-particle–light-particle correlations

It has been suggested[32] that the angular correlations between light particles emitted in the compound nucleus decay are sensitive to the angular momentum in the entrance channel. In particular, for the reactions $^{16}O+^{27}Al$, $^{nat}Ca$, and $^{58}Ni$ at 50–70 MeV bombarding energies, the $\alpha$-$\alpha$ correlation with in-plane geometry ($\Delta\phi=180°$) selects mainly events coming from high spin states, whereas an out-of-plane geometry ($\Delta\phi=90°$) has contributions from all angular momenta.

We have made a comparison between the experimental spectra for light particle correlations in the $^{32}S+^{27}Al$ reaction and those calculated by the Monte Carlo version of CASCADE which describes so accurately the single energy spectra of protons and alpha particles. These Monte Carlo calculations for two-particle correlations are extremely time consuming: the calculations reported in the following involve $10^5$ histories for each data set and needed $\sim 100$ cpu hours on a 8600 VAX computer.

The comparisons between the experimental data and the Monte Carlo simulations are reported in Fig. 9 and in Table III. The statistical model generally describes well the experimental data for $\alpha$-$\alpha$, $\alpha$-$p$, and $p$-$p$ coincidences showing that this type of calculation reproduces a variety of observables associated with the decay of the Cu compound nucleus, even that resulting from a well-defined subset of deexcitation paths in the case of two-particle correlations. Set 2 appears to provide a somewhat better description of these correlations.

We have extracted from the Monte Carlo calculation the average spin of the events populating singles and coincidence spectra to verify the selectivity of the $\alpha$-$\alpha$ correlation. Data are reported in Table IV. At this ener-

TABLE IV. Average spin values of the events yielding light-particle–light-particle correlations in the Monte Carlo statistical model calculation. The corresponding value for $\alpha$ singles is reported for comparison. $E_{beam}=150$ MeV; $\theta_1=\theta_2=60°$; $\Delta\phi=180°$.

| Type of correlation | Set 1 mean $J$ ($\hbar$) | Set 2 mean $J$ ($\hbar$) |
|---|---|---|
| $p$-$p_{coincidences}$ | 18.8 | 18.9 |
| $\alpha$-$p_{coincidences}$ | 24.6 | 25.4 |
| $\alpha$-$\alpha_{coincidences}$ | 31.0 | 27.6 |
| $\alpha_{singles}$ | 24.6 | 24.7 |

gy the mean angular momentum of the compound nucleus spin distribution is $26\hbar$. Set 1 results show also for the $^{32}S+^{27}Al$ reaction the predicted enhancement of the spin (mean $J$ is $\sim 31\hbar$) for the states populating the $\alpha$-$\alpha$ channel with the in-plane geometry. This spin selection is less evident in the set 2 calculation (mean $J$ is $\sim 28\hbar$) as a consequence of the lower alpha emission from the high spin states in the first step of deexcitation. This dumping produces a lower probability of $\alpha$-$\alpha$ events from high spin reducing the differences in average spin between singles and coincidences.

### D. Deuteron and triton evaporation

The evaporation of deuterons ($d$) and tritons ($t$), though relatively rare at these bombarding energies, may provide further information on the deexcitation of the compound nucleus. In the present experiment, the $d/p$ ratio ranges from $1.5\times10^{-2}$ to $2.7\times10^{-2}$ at $\theta_{lab}=30°$ for bombarding energies from 100 to 150 MeV, the $t/p$ ratio from $1\times10^{-3}$ to $2.3\times10^{-3}$.

The small cross section is essentially explained by the higher binding energy $S$ of $d$ and $t$ in $^{59}Cu$ with respect to

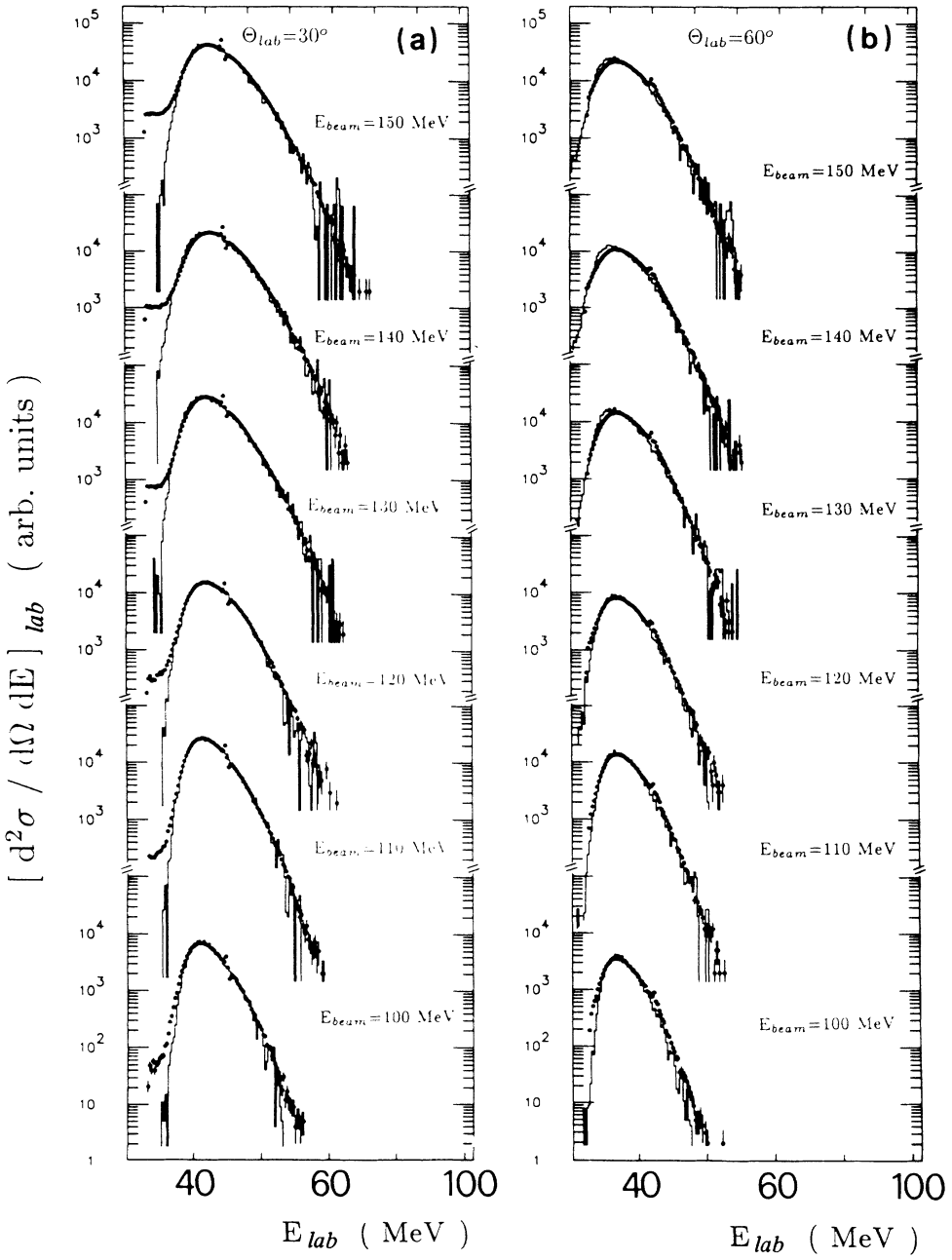


FIG. 4. Experimental and calculated alpha particle spectra for 100–150 MeV bombarding energies at $\theta_{lab}=30°$ (a), 60° (b), 120° (c), 150° (d). Calculations are standard statistical model (set 2) using the CACARIZO code.

that of $p$ ($S_p = 3.4$ MeV, $S_d = 13.4$ MeV, and $S_t = 17.4$ MeV). Considering H isotopes evaporated with the same kinetic energy, the $d$ and $t$ are sensitive to a level density in the daughter nucleus $\sim 10$ MeV lower in excitation energy than $p$ producing the ratio $10^{-2}, 10^{-3}$ in yield at the excitation energies involved in this work.

The binding energies of $d$ and $t$ in nuclei populated after $n$, $p$, and $\alpha$ emission from the $^{59}$Cu are, respectively, 1.4 and 3.3 MeV larger on the average than those in the $^{59}$Cu itself so that the emission of heavy H isotopes in the second step of the deexcitation is further inhibited. When $d$ and $t$ emission is included, the model calculations predict that the probabilities that the observed $d$ and $t$ are emitted in the first step of the decay are $\frac{1}{2}$ and $\frac{3}{4}$, respectively, to be compared with $\frac{1}{5}$ for $n$ and $p$ and $\frac{1}{3}$ for alpha particles. At 150 MeV bombarding energy, the mean angular momentum of the states decaying by $d$ and $t$ emission is predicted to be $\sim 21\hbar$ and $\sim 24\hbar$, respectively. The $d$ and $t$ should then be a sensitive probe to the structure of the compound nucleus at the starting point of the deexcitation.

Figure 10 shows the center-of-mass deuteron spectra compared with the CASCADE calculation using set 1 (a) and set 2 (b) input parameters. The deuteron transmis-

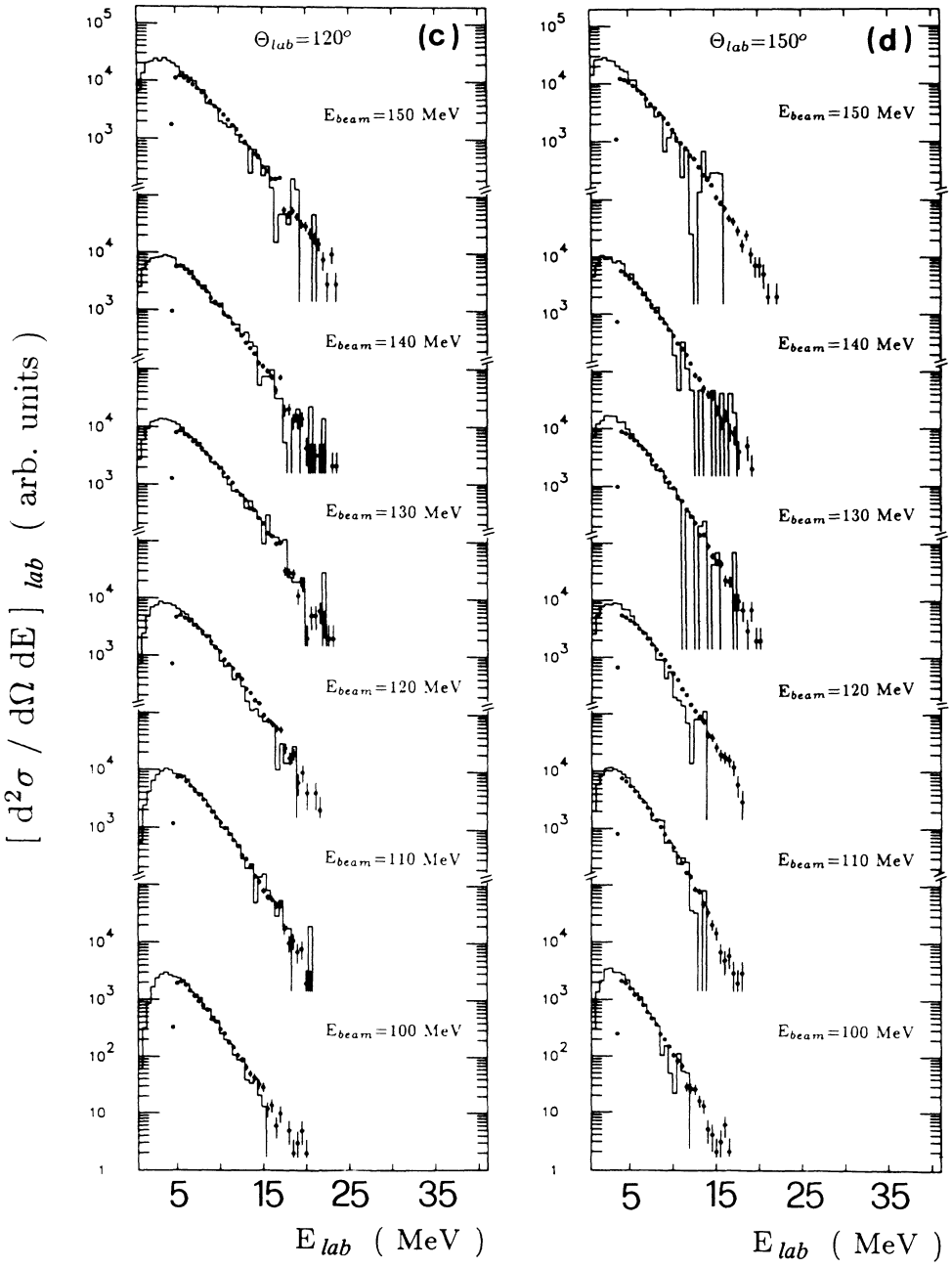


FIG. 4. (*Continued*).

sion coefficients are from Ref. 33. Deuteron spectra appear more sensitive than the proton spectra to the input of the model calculations and show the same trend with the bombarding energy found in the case of $\alpha$ particles.

Data for tritons at 150 MeV are shown in Fig. 11. The same considerations outlined for deuterons hold in the triton case with a larger sensitivity to the input of the model calculation. Transmission coefficients for tritons are from Ref. 34.

In the calculations of Figs. 10 and 11 the transmission coefficients for $d$ and $t$ were computed using the RFACT values as determined from $p$ and alpha singles.

## IV. DISCUSSION

As shown in the preceding section, the statistical model calculation is capable of describing several aspects of the deexcitation of the compound nucleus $^{59}$Cu but adjustments are required in $T_l$ and yrast energies as the bombarding energy exceeds 100 MeV.

By changing the bombarding energy from 100 to 150 MeV, the nuclear temperature $T$ is increased only from 2.4 to 2.7 MeV (considering the RLDM yrast of Fig. 1). The maximum spin rises from 27 to 36$\hbar$. It is assumed that the adjustments in the model calculation are mainly

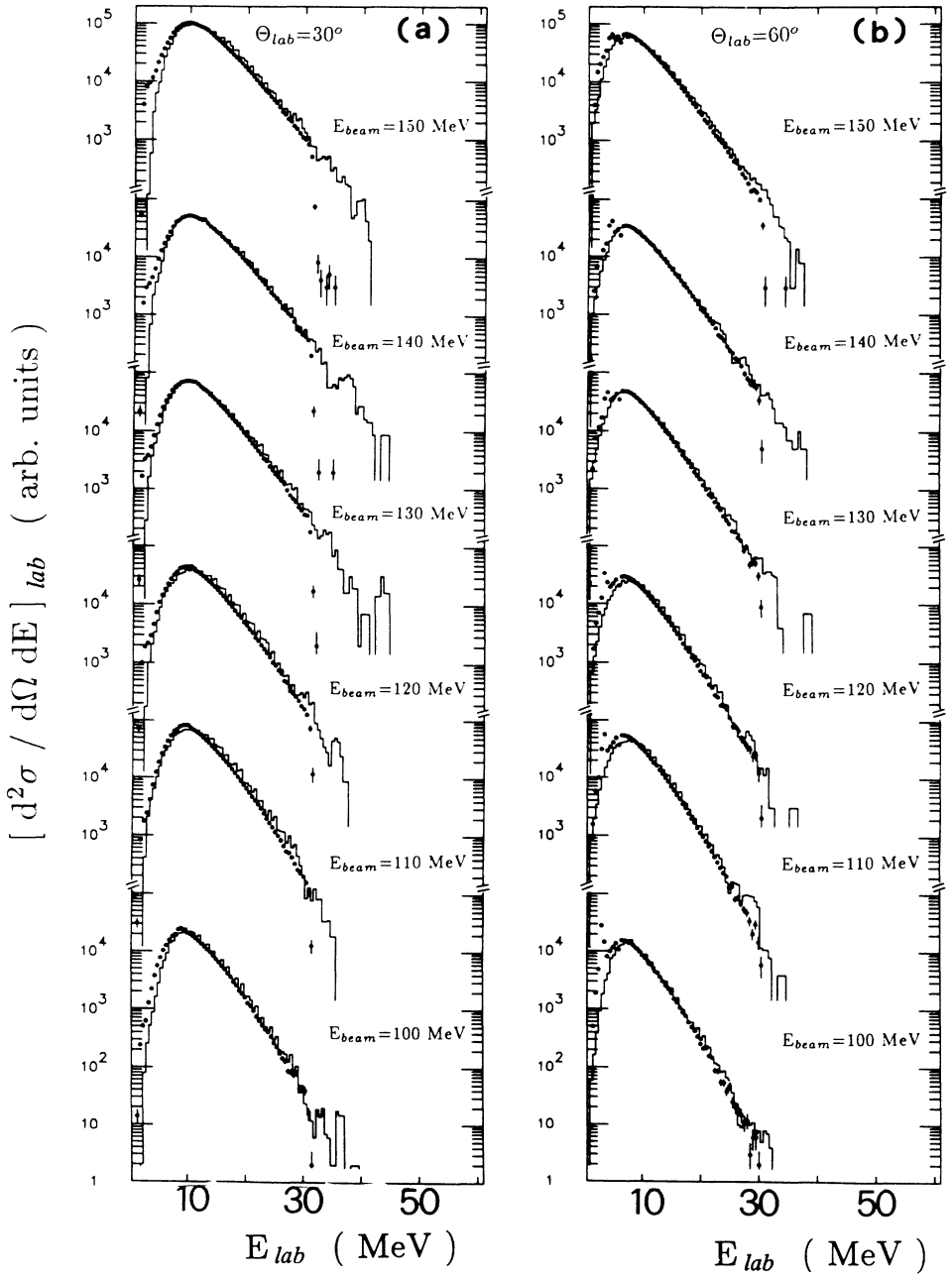


FIG. 5. As Fig. 4 but for protons.

required because of the spin change. Following the RLDM predictions,[5] the compound nucleus can be considered as spherical or slightly deformed at the lower bombarding energy, becoming strongly deformed as the spin increases. The RLDM predicts moderate oblate deformations for $A=59$ nuclei at spins above $30\hbar$. A strong prolate deformation is predicted for spin values larger than $J\sim 40\hbar$.

### A. Transmission coefficients and effective emission barriers

The transmission coefficients play an essential role in the statistical model calculations. Optical model potentials are normally used for the evaluation of the inverse transition probabilities and cross sections.

In the case of nucleons, the transmission coefficients describe (1) the penetration of the particles through the Coulomb and centrifugal barriers; (2) the reflection at the nuclear surface; (3) the resonances within the nuclear potential.

The optical model parameters carry essential information on the shell structure of the target (daughter) nucleus in the scattering (emission) process. As an example, the size resonances exhibited by the nucleon-nucleus absorption cross sections are determined primarily by low-energy transmission functions.

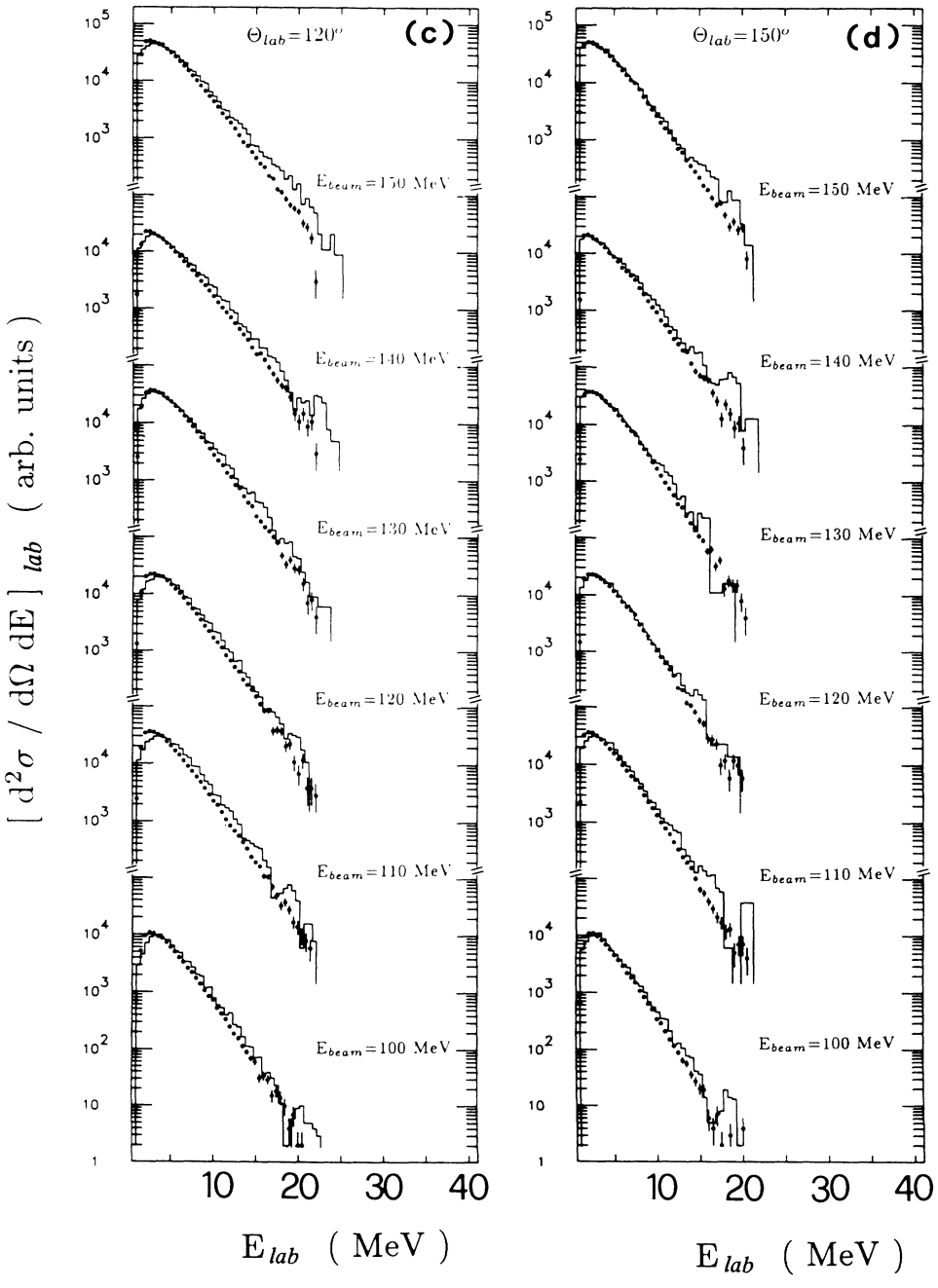


FIG. 5. (*Continued*).

For $d$, $t$, $\alpha$, or heavy clusters the size resonance is absent because these particles are more strongly absorbed. Therefore, the transmission coefficients are not sensitive to the depth of the optical potential and are very near those of the "black nucleus" multiplied by the appropriate reflection factor.[1]

Figure 12 shows the effective barriers $B_l$, defined as the energy at which $T_l=0.5$, as a function of the particle angular momentum for $p$, $d$, $t$, and $\alpha$. The $B_l$ values are calculated from the optical model parameters for spherical nuclei (i.e., with RFACT=1). The effective barrier for protons fluctuates and is very steep with $l$ while those for heavier particles have a smooth and weak dependence on the angular momentum.

The trend of $B_l$ with angular momentum suggests that protons are emitted essentially with low $l$ while the other particles may carry sizable angular momentum.

The effective barriers from OM potentials for the $s$-wave particles, $B_{l=0}$, are 4.8, 4.3, and 4.2 MeV for $p$, $d$, $t$, and 6.9 MeV for $\alpha$. Those values may be compared with the values 4.8 and 8.5 MeV for $p$ and $\alpha$, respectively, from the Vaz and Alexander compilation of empirical fusion barriers.[35]

It has been shown that for $A=50-60$ nuclei, this "empirical fusion barrier" determined from excitation functions is higher than that derived from the evaporation spectra. As an example, the spectra of evaporated alpha particles from Co, Ni, and Cu compound nuclei, populated at low spin and excitation energies in proton or alpha induced reactions, peak at $\sim 8.5$ MeV.[29] The peak energies of evaporation spectra are expected to be larger than the barrier energies. The barrier evaluated from the evaporation spectrum is, in fact, 7.2 MeV,[35] in fair agree-

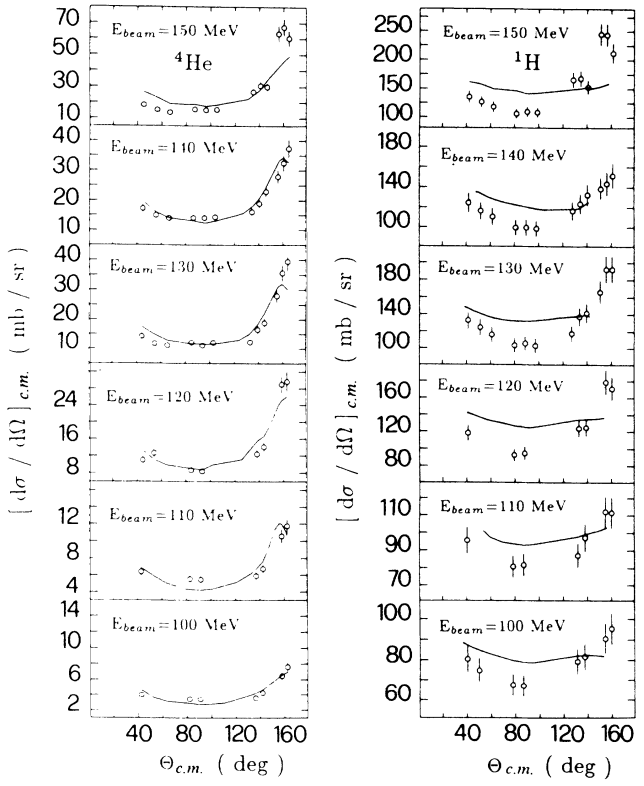


FIG. 6. Experimental and calculated angular distributions for protons and alpha particles. The low-energy thresholds are 17 and 5 MeV for alpha and protons, respectively. Calculations are from CACARIZO code using the set 2 parameters.

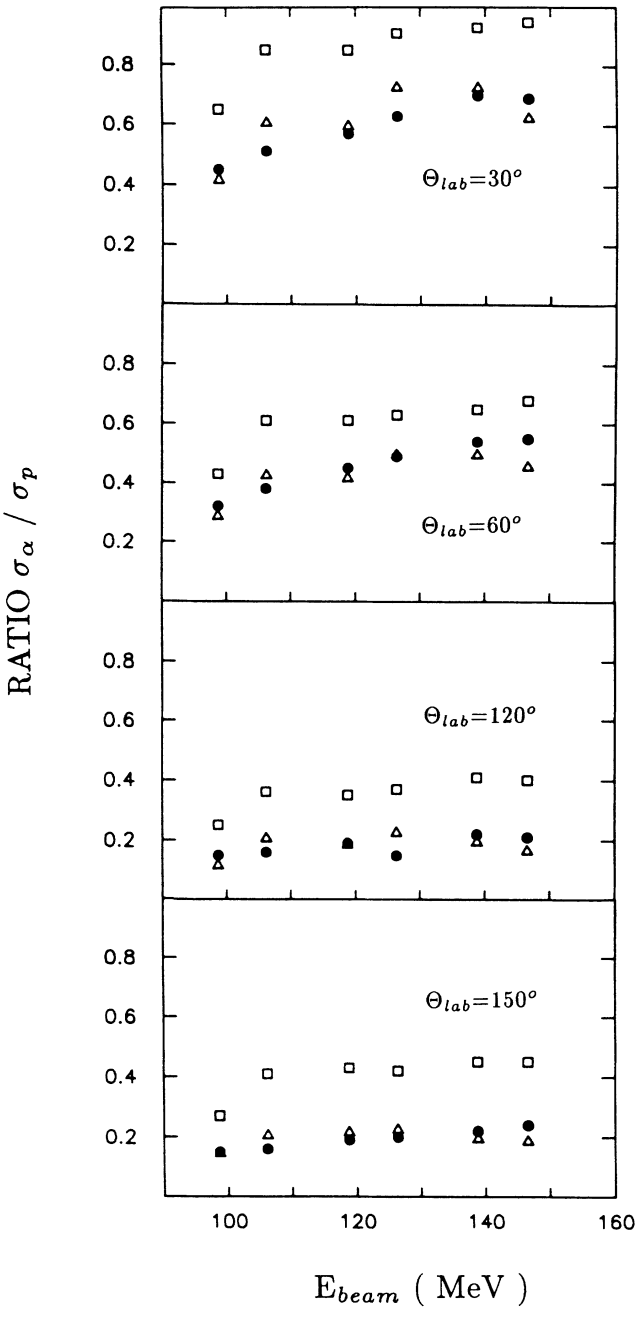


FIG. 7. Experimental (solid points) and calculated alpha-to-proton ratio for 100–150 MeV bombarding energies at $\theta_{lab}=30°, 60°, 120°, 150°$. Calculations are standard statistical model using the CACARIZO code. The triangles refer to the set 2 input data, the squares to the set 1 ones.

ment with that from the OM. Furthermore, evaporative calculations using the same OM potentials for alpha particles as in this work reproduce the excitation functions of $\alpha$ induced reactions[35] and the spectral shape of evaporated particles[36] for $A = 50-60$ nuclei.

The OM $\alpha$ potentials used to compute transmission coefficients seem to describe reasonably well several aspects of the evaporation from nuclei in this mass region for reactions at low spin, in agreement with the good description of the spectral shape obtained for the 100 MeV $^{32}$S+$^{27}$Al reaction.

One of the long-standing problems in the statistical model is that no information is available on the optical model parameters appropriate for calculating the transmission coefficients of excited states populated in the compound nucleus. This problem becomes extremely important in the case of heavy-ion induced reactions because of the thermal and dynamical deformations of the hot rotating nucleus and the corresponding shape fluctuations suffered during the cooling process. This might justify *ad hoc* adjustments of the optical model parameters. The experimental guidance for transmission coefficient adjustments is the lower energy portion of the particle spectrum, sensitive to the effective barrier of the particle-nucleus system.

At higher bombarding energy, the optical model radius is increased to lower the emission barrier for alpha particles. By using RFACT=1.25 at 150 MeV, the $B_{l=0}$ for alpha emission is reduced by $\sim$20% to 5.4 MeV. This reduction, needed to reproduce the data at the higher energy, is larger than that reported for the 240 MeV $^{40}$Ar+$^{27}$Al ($\sim$8%, see Table II in Ref. 17). We note that this latter represents an average lowering for all the spin values contributing to the alpha, the dynamical induced deformation should lower the barrier in a spin dependent way. In fact, as determined by an unfolding procedure, the barrier lowering for the 240 MeV $^{49}$Ar+$^{27}$Al system at $J = 40-50\hbar$ was also found to be $\sim$20%.

With RFACT=1.25, the effective barrier for protons is increased by 0.5 MeV, instead of decreasing as the alpha barrier. This is related to the different meaning of transmission function for nucleon and cluster as discussed above.

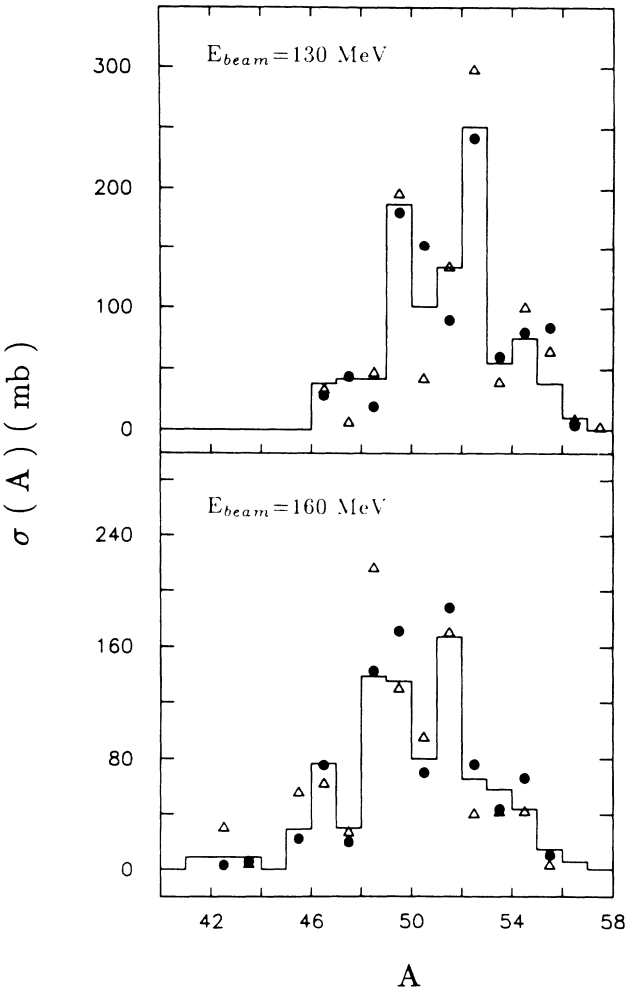


FIG. 8. Experimental (histogram) and calculated evaporation residues distributions from the $^{32}$S+$^{27}$Al reaction at 130 and 160 MeV. Statistical model calculation are from the CASCADE code using the set 1 (triangles) and the set 2 (dots) input data.

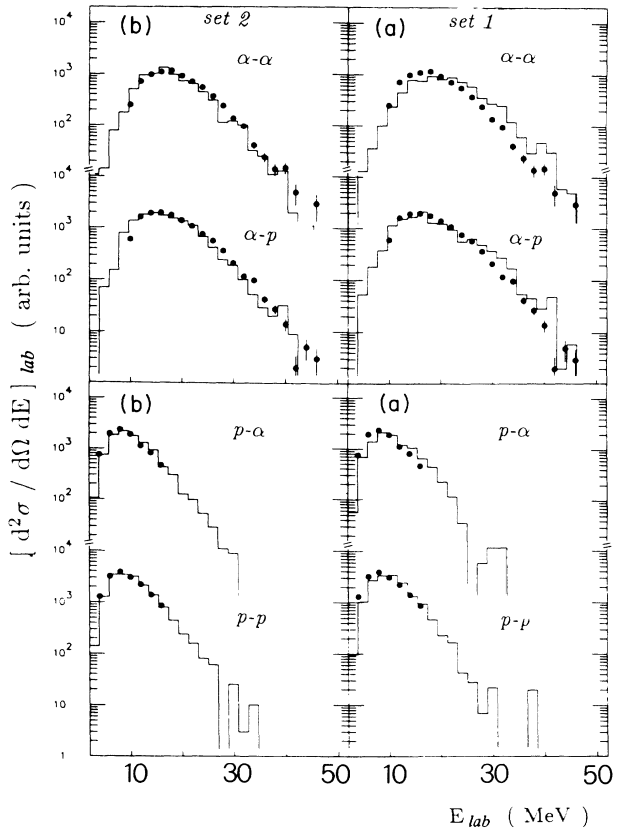


FIG. 9. Experimental and calculated light-particle–light-particle correlations at 150 MeV bombarding energy at $\theta_{lab1} = \theta_{lab2} = 60°$, $\Delta\phi = 180°$. The energy spectra refers to the first particle of each correlation. Statistical model calculation are from the CACARIZO code using the set 1 (a) and the set 2 (b) input data.

The effect of deformation on the transmission coefficients has been discussed in detail by Blann.[9] In that work the lowering of the barrier, which occurs for any angular momentum $l$, lead not only to an increased yield of low energy particles, but also to an extra production of energetic particles carrying away more angular momentum, i.e., to an "amplification factor" in the energy spectra.

To clarify the link between the Blann predictions and the procedure used in this work, we show in Fig. 13 the $T_l$'s versus $l$ for the emission of 10, 20, and 30 MeV alpha particles calculated from the OM potential for spherical (RFACT=1) and deformed (RFACT=1.25) nuclei. The opening of the phase space for the emission of alphas at higher $l$ appears clearly. As a consequence of the change in the $T_l$, the shape of the particle spectrum is changed.

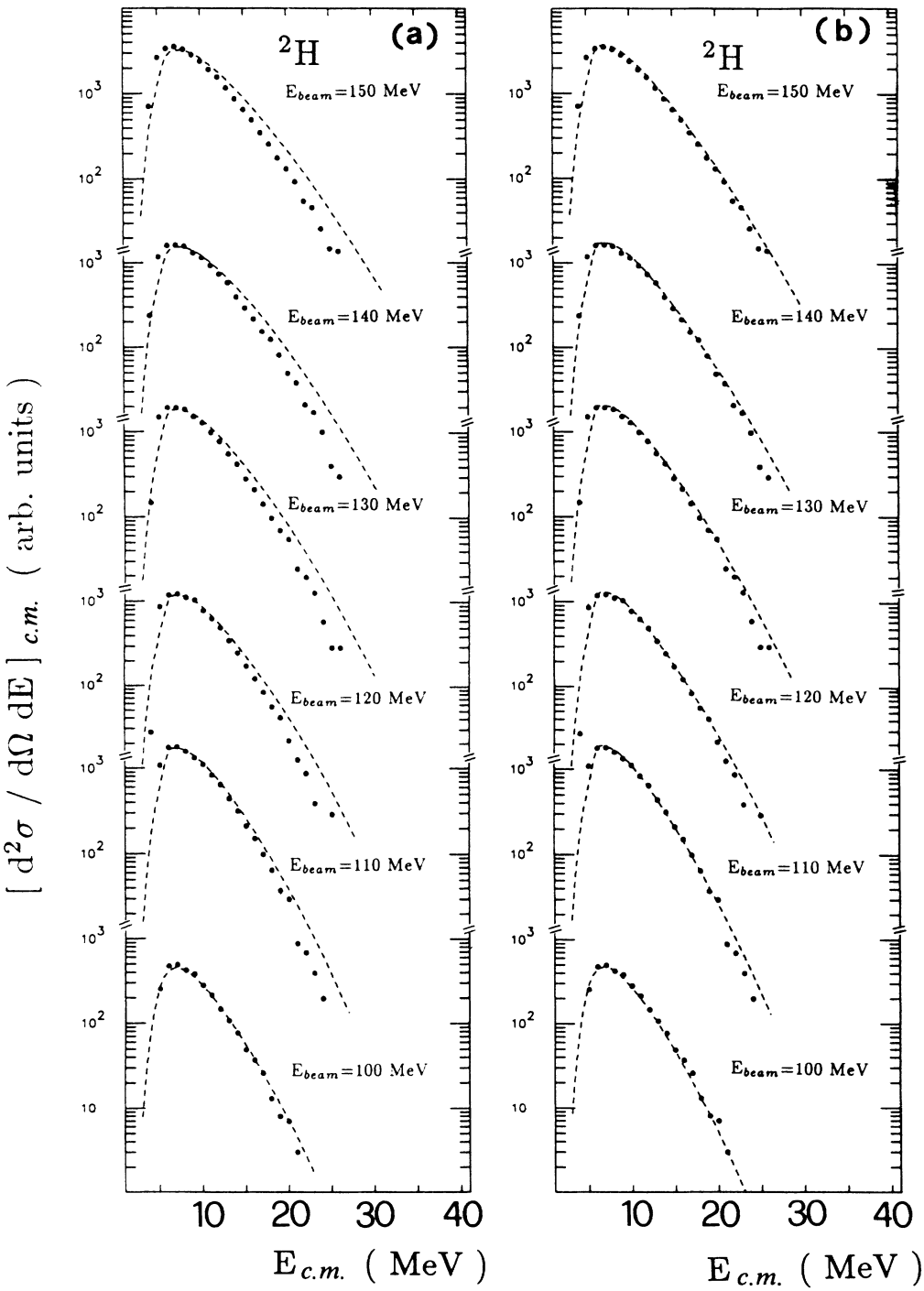


FIG. 10. COM converted deuteron spectra (100–150 MeV bombarding energy, $\theta_{lab}=30°$) compared with CASCADE calculations using the set 1 (a) and set 2 (b) input data.

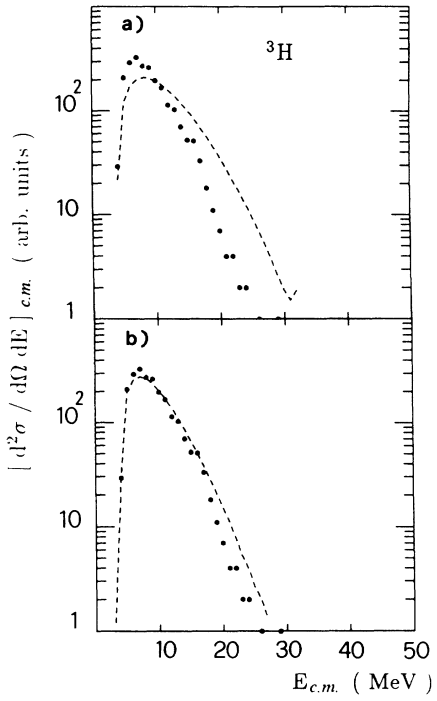


FIG. 11. COM converted tritium spectra (150 MeV bombarding energy, $\theta_{lab}=30°$) compared with CASCADE calculations using the set 1 (a) and set 2 (b) input data.

This is shown in Fig. 14 for alphas and protons, respectively. We notice once again that the proton spectra are quite insensitive to the radius changes.

The change in $T_l$ alone, which leads to the amplification factor predicted by Blann, does not explain the deviation between experimental and calculated spectra shown in Fig. 1 because in this way the production of energetic particles is increased. On the contrary, our data show that the production of high-energy $\alpha$ particles

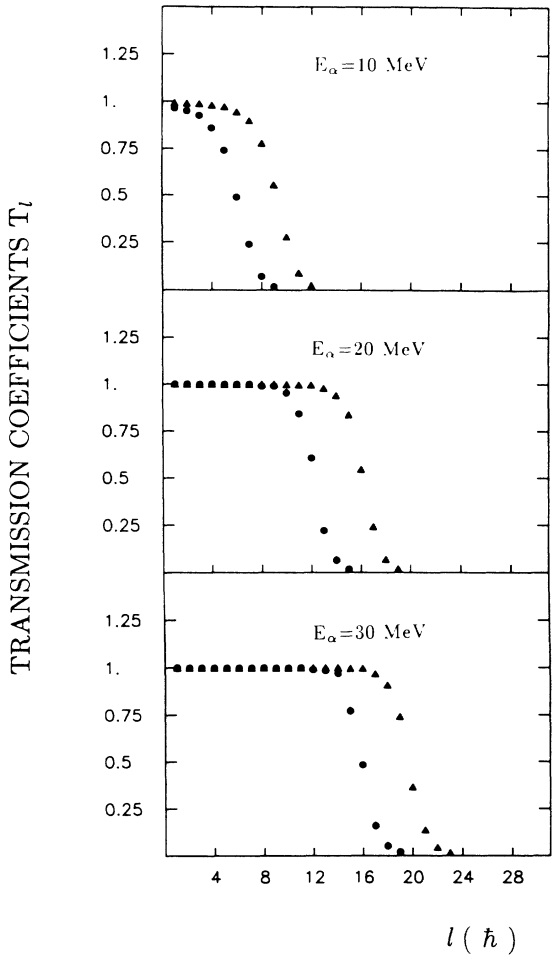


FIG. 13. Transmission coefficients $T_l$ vs the spin $l$ for the emission of 10, 20, 30 MeV $\alpha$ particles for OM potentials using standard radius values (points) and increased (RFACT=1.3) values (triangles).

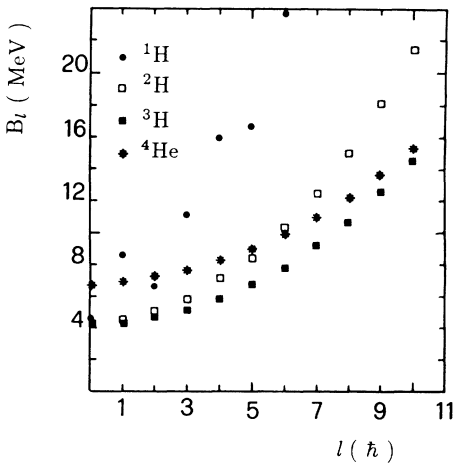


FIG. 12. Effective barrier vs spin value for $p$, $d$, $t$, $\alpha$ from the OM standard potentials for spherical nuclei (RFACT=1).

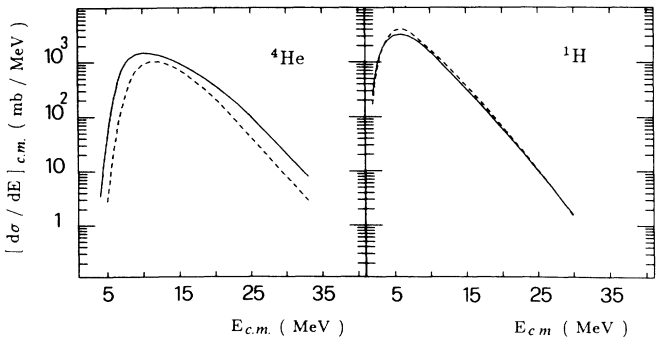


FIG. 14. Amplification of the particle spectra by changing the $T_l$ coefficients. CASCADE calculation for 150 MeV bombarding energy using the set 1 input data and $T_l$ coefficients from OM potentials with standard radius value (dashed line) and increased (RFACT=1.3) value (solid line).

is lower than predicted in the standard statistical model and an additional modification to the model is required to explain the observation. We turn to the question of yrast lines and level densities to explore this additional factor.

### B. Yrast line and level density

As shown in Sec. III, the high-energy tails of the light particle spectra are well reproduced by the statistical model calculation if the position of the yrast line is changed in a spin dependent way. The position of the yrast line in the $(E_x,J)$ plane depends on the average shape of the nucleus rotating with spin $J$ which determines the energy tied up as deformation energy and, through the moment of inertia, the rotational energy. The available predictions on the shape of a $A=59$ nucleus, from the RLDM of Cohen, Plasil, and Swiatecki[5] to the recent works of Sierk[26] and Mustafa,[25] yield collective lines which are close to that used in the set 1.

The adjusted yrast line used to reproduce the spectra (set 2), lies well below the lines predicted by theory. As discussed in Ref. 17, the need in the calculation of this lower yrast line does not imply that nuclei are more deformed than predicted by theory. The CASCADE code, as the majority of the available computer codes, does not treat the deformation in a complete and consistent way. The codes consider the RLDM yrast line reflecting deformation increases with the spin, but the level density at any $J$ is that appropriate for a spherical nucleus (the Lang formula) with excitation energy $E=E^*-E_{\text{yrast}}$.

The empirical progressive lowering of the yrast as a function of $J$ increases the number of levels available at a given excitation energy at high spin. Indeed an enhancement of the level density due to the nuclear deformation is predicted in the framework of several different models.

Toke and Swiatecki[37] have derived, using the Thomas-Fermi treatment and the leptodermous expansion, a prescription for the level density parameter $a$ which takes into account the diffuse surface region due to the deformed nuclear shapes. Applying this treatment to the present case, the predicted enhancement is quite low ($\sim 1.2$) using either RLDM or two-center-model predicted shapes.[5,25]

Recently Barranco *et al.*[38] have calculated the effect of the quadrupole deformation on the nuclear level density parameter $a$ for axially symmetric shapes. Enhancements similar to those calculated by Toke and Swiatecki are found.

Bjornholm, Bohr, and Mottelson[3] showed that in nuclei having static deformations, the level density is appreciably greater than for spherical nuclei because of the contribution of the low-energy rotational levels. The magnitude of this effect depends on the symmetry of the nuclear shape, which determines the collective rotational degrees of freedom. Comparing the experimental level density with calculations for spherical nuclei, an enhancement of 60–100 in case of statically deformed nuclei at low excitation and spin has been deduced.[7,8] The effect of including this collective enhancement of the level density in statistical model calculation has been discussed by Vigdor and Karwowski.[6]

From a qualitative point of view, the expected enhancement of the level density driven by the deformation might account for the required yrast line lowering when a level density formulation for spherical nuclei is used in the calculation. An explicit inclusion in the calculation of level densities for deformed nuclei is clearly indicated. This task appears to be quite difficult in the present case because the available formulations of level densities for deformed nuclei are valid only in the limits of small values of spin and rotational energy ($E_{\text{rot}} \ll T$).[7,9,39] If this condition is not fulfilled as for the $^{32}\text{S}+^{27}\text{Al}$ reactions, the use of this formulas leads to a level density at high spin ($J=30-40\hbar$) which is close to or even lower than the spherical case.

It is also expected that the collective enhancement predicted by Bjornholm, Bohr, and Mottelson should disappear at high temperature with the weakening of the shell structure due to the thermal fluctuation.

### C. Level densities and barriers at high spin

The information obtained about the evaporation barrier and the level densities in the Secs. IV A and IV B is limited because it is derived by comparing the total emission spectra with calculations including contributions from all spins and decay steps. In this section we try to go beyond this averaging by isolating the emission from those regions of angular momenta for which large deformations are predicted.

Experimentally, spectra are obtained by measuring excitation functions which span increasing angular momentum windows and increasing excitation energies. To obtain the spectra associated with high spin windows, the contribution of the low spin has to be subtracted from the total emission spectrum at fixed excitation energy. To explore this question further the most useful spectra would be angle integrated COM spectra. The experimental thresholds at backward angles prevent such a complete spectrum from being reconstructed. Thus we began by ascertaining the extent to which the laboratory spectra at particular angles are representative of the total spectrum, i.e., free from spin fractionation effects.

This point was investigated by first comparing the shape of the center-of-mass converted energy spectra of the alpha particles detected at angles $\theta_{\text{lab}}=30-120°$. These spectra agree very well with each other. A further test was made by comparison with the model calculations. The CASCADE program outputs the integrated COM energy spectra of the evaporated particles. Angular distribution effects are explicitly considered in the Monte Carlo kinematical simulation CACARIZO (set 2 input) which describes very well the alpha spectra. This simulation predicts that the differences in the average spin contributing to alpha spectra taken at different laboratory angles around $\theta_{\text{c.m.}}=90°$ are low (on average $\sim 1\hbar$). Consequently we observe that the shapes of laboratory spectra simulated by CACARIZO coincide, once converted in the COM system, with the summed evaporation spectra of CASCADE.

We conclude that the measured spectra taken at fixed laboratory angle around $\theta_{\text{c.m.}}=90°$ are equivalent to the

spectra from the entire spin distribution of the fusion reaction. Therefore, we used the experimental spectra taken at $\theta_{lab}=30°$ which have the lowest experimental thresholds to represent the angle integrated spectrum.

For "low spins" spectra we assumed that the statistical model with the standard parameters (set 1) which describes well the decay of $^{59}$Cu up to $27\hbar$ at $E_x=59$ MeV excitation, will do as well for the same spin range at the higher excitation energies (up to $E_x=81$ MeV corresponding to the 150 MeV irradiation). As reported recently, the study of the decay of the giant dipole resonance in excited $^{63}$Cu has shown that such nuclei are close to the ground-state shape in a range of spin and excitation energies comparable with the present "low spin" definition.[40] The high-energy $\gamma$ ray spectra in that work are well described by standard CASCADE calculations.

We have therefore calculated using the set 1 parameters the spectra associated with the low spin values ($0-27\hbar$) at the excitation energies corresponding to the 110 to 150 MeV irradiations and subtracted these spectra from the experimental ones. Figure 15 shows an example of this subtraction procedure.

In Table V are reported the average values $J_{ave}$ of the angular momentum windows obtained in this way. Figure 16 shows the resultant difference spectrum for each bombarding energy compared again with the standard calculations (set 1). The high spin selection emphasizes the difference between the experimental spectra and the standard calculations at low as well as at high alpha energy. The role of the emission barrier and level densities can now be studied as a function of different average spin $J_{ave}$ at slightly changing excitation energies above the yrast line.

Also reported in Fig. 16 are the results of the model calculations using the set 2 input data. Both the spectral shape and the absolute cross sections for $\alpha$ emission are well described when the adjustments are made. The lowering of the barrier is essential in describing not only the low-energy part of the spectra, but also the cross section for alpha emission.

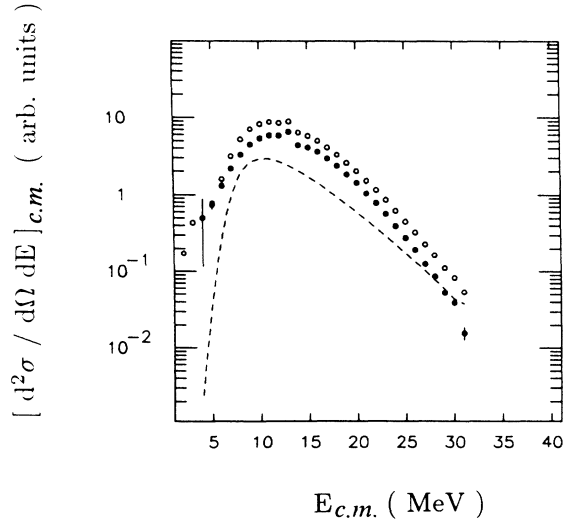


FIG. 15. Example of subtraction procedure to obtain the high spin alpha spectra at 150 MeV bombarding energy. The open dots refer to the measured spectrum, the broken line is the calculated low spin spectrum, and the black dots are the resultant difference spectrum.

TABLE V. Summary of the high-spin alpha spectra analysis.

| $E_{beam}$ (MeV) | $J_{ave}$[a] ($\hbar$) | $B_\alpha/B_{\alpha,sph}$[b] | $\Delta E$[c] (MeV) | $\rho_{exp}/\rho_0$[d] |
|---|---|---|---|---|
| 100 | | 1 | | |
| 110 | 28.0 | 0.96 | 5.2 | 12 |
| 120 | 29.5 | 0.92 | 6.2 | 22 |
| 130 | 32.3 | 0.88 | 8.5 | 46 |
| 140 | 32.8 | 0.83 | 8.9 | 68 |
| 150 | 34.2 | 0.81 | 10.2 | 95 |

[a]Average spin value associated with the spin window from $27\hbar$ to $J_{max}$ (see Table I).
[b]Fractional barrier relative to that of a spherical nucleus. The barrier lowering is obtained by increasing the radius values in the OM potentials.
[c]Excitation energy increase due to the lowering of the yrast line at $J=J_{ave}$.
[d]Enhancement factor in the level density at $J=J_{ave}$ and 17 MeV excitation above the RLDM yrast line. Estimated uncertainties are a factor of 2.

We report in Table V, for each value of the average spin $J_{ave}$ the excitation energy increment, $\Delta E$, resulting from the lowering of the yrast line which is needed to reproduce the experimental data of Fig. 16.

Assuming that this effect is totally due to the fault in calculating level densities, the $\Delta E(J)$ can be converted into "experimental" level density using the Lang formula for an excitation energy $E_x-E_{yrast}(J)+\Delta E(J)$. Therefore, it is possible to estimate the enhancement factor of the "experimental" level density relative to that of the spherical nucleus [Lang formula at excitation energy $E_x-E_{yrast}(J)$] and its dependence on the spin. Because in this experiment the different spin $J_{ave}$ refers to slightly different excitation energies (different bombarding energies), the enhancement factor is reported in Table V for a value of 17 MeV excitation above the RLDM yrast line which is an average value for the residual nucleus after the emission of alpha particles from the high spin windows. We note that slightly different yrast lines reproduce the data reasonably well, with $\Delta E$ values varying by $\sim 1.8$ MeV. This gives an uncertainty of a factor 2 on the level density enhancement factor.

In Table V we report also the values of the fractional barrier for $l=0$ alpha emission associated with the radius change in the optical model potential.

As shown also Fig. 15 is the major fraction of the low-energy particles derived from the decay of the high spin states, so that the average barrier reduction needed to reproduce the high spin spectra practically coincides with those deduced from the total evaporation spectra.

We can now compare this barrier reduction and the radius multiplication factor with that predicted by theory. This is done in Fig. 17 where the experimental fractional

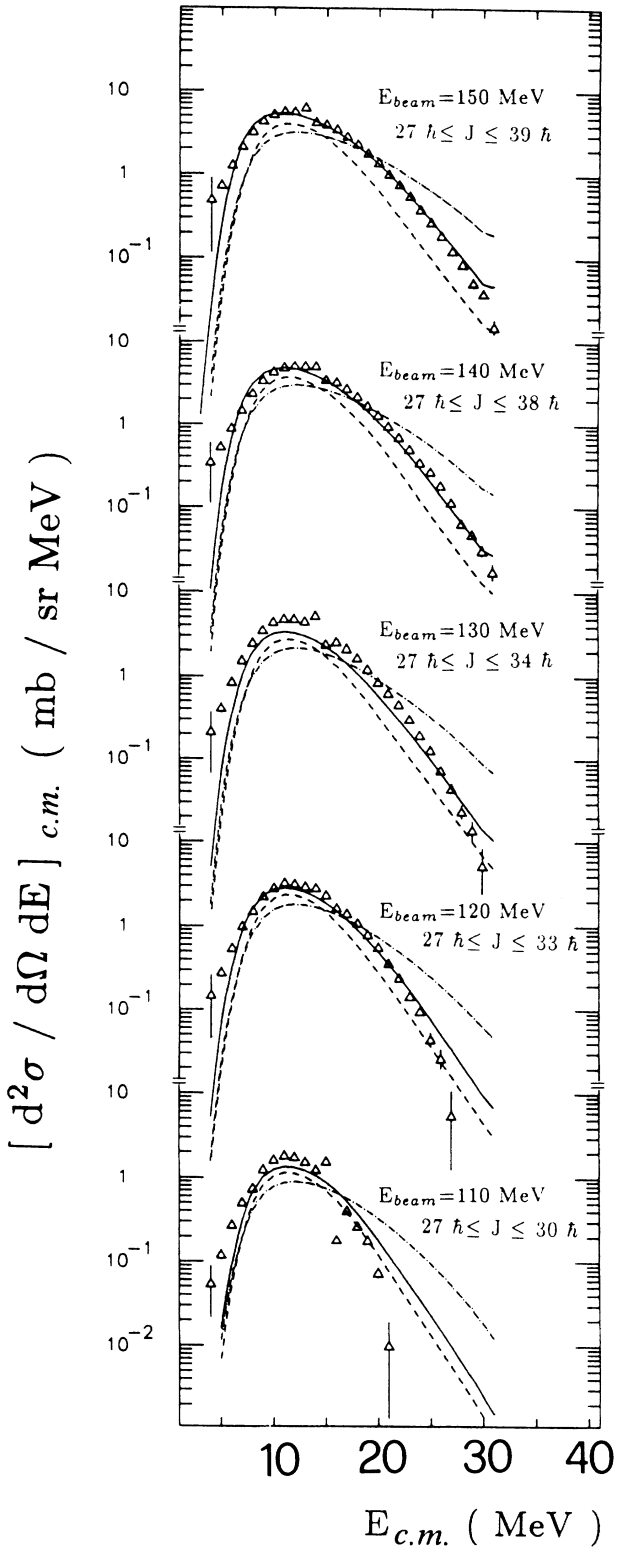


FIG. 16. Comparison of resultant center-of-mass spectra of alpha particles after subtraction of the low spin and calculated CASCADE spectra using set 1 input parameters (dash-dotted line) or the set 2 ones: yrast line lowered (dashed line), yrast line lowered and barrier reduced (solid line).

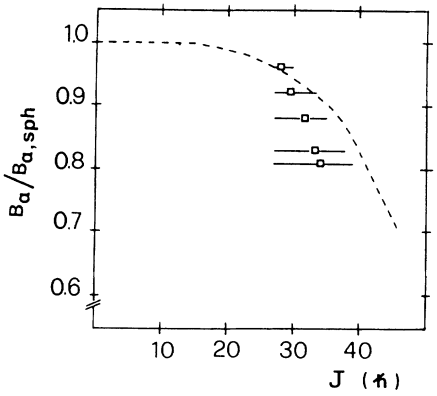


FIG. 17. Comparison of the fractional barrier lowering determined from the high spin alpha spectra and that calculated by Blann (Ref. 9) by numerical integration of sharp cutoff transmission coefficient over the nuclear shape predicted by RLDM.

barriers are compared directly with those calculated by Blann[9] by integrating sharp cutoff transmission coefficients on the surface of a deformed nucleus with $A=56$ assuming RLDM shapes. The barrier reduction extracted from the experimental data is larger than that calculated at the higher spin. This is because the corresponding radius multiplication factor, necessary to fit the data, is RFACT=1.25, practically equal to the ratio of the major axis to the spherical radius for the nuclear shape predicted by the RLDM.[5] The Blann calculation, integrating the barrier over the entire surface, yields an average barrier which is higher than that corresponding to the emission along the major axis only, i.e., from the tips of the ellipsoid.

One can raise the question of the sensitivity of the high spin spectra on the determination of the low spin emission. In fact, the set 2 input which describes the lowest bombarding energy data better, would produce slightly

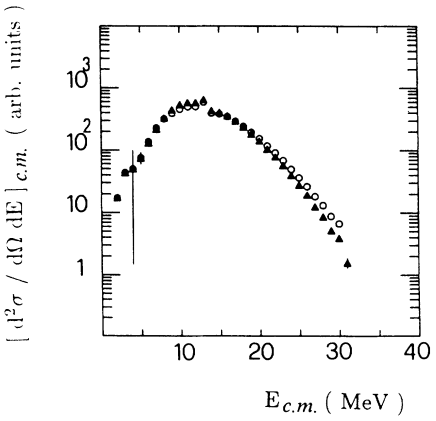


FIG. 18. Example of high spin spectra obtained at 150 MeV bombarding energy subtracting from the experimental spectrum different low spin calculated contributions (set 1 triangles, set 2 dots).

different low spin spectra because of the small difference in yrast line around $J=27\hbar$. At 130–150 MeV bombarding energies, the states of initial angular momentum $J \geq 27\hbar$ strongly contribute to the alpha spectrum. The subtraction of the low spin contribution with set 1 or set 2 input data, produces resultant spectra very close one to the other as shown in Fig. 18. This assures that for these high spin windows the uncertainties in the derivation of the barrier and level density enhancement are scarcely dependent on the subtraction procedure.

## V. CONCLUSIONS

We have measured energy spectra and angular distributions of the light particle $(p,d,t,\alpha)$ emitted in the decay of the $^{59}$Cu formed in the reaction of $^{32}S+^{27}Al$ at 100 to 150 MeV bombarding energies. Light-particle–light-particle correlations have been also measured at the higher bombarding energy. These experimental data, linked with the published fusion cross sections[15] and evaporation residue distributions,[12,13] constitute a detailed information to establish the validity of the statistical model for these excitation energies and spins and to explore the structure of the hot rotating compound nucleus.

We found that standard statistical model calculations, performed with the computer code CASCADE and CACARIZO generally describe well the experimental data at the lowest bombarding energy. This is in agreement with previous experiments observing light particles[11,17] and high-energy $\gamma$ rays[39] in this mass region. Increasing deviations are found between the experimental data and the standard calculation at higher bombarding energies. Model calculations with adjusted emission barriers and level densities are able to describe the experiment. The magnitudes of the required adjustments are supposed to be associated with deformation effects.

To correlate the needed adjustments with well-defined deformations, we have isolated the emission from narrow windows of angular momentum by a subtraction procedure based on the hypothesis that the standard calculation accounts well for the low spin region. By comparing these "high spin" alpha spectra with the model calculation we are able to derive from each spin window the required emission barrier lowering and level density enhancement.

The parameter adjustments needed to reproduce the experimental data seem to be consistent with theoretical expectations for hot rotating nuclei. The fractional barrier lowering resulting from the adjustment of the calculation to the experimental data is 20%, obtained by increasing the radius in the OM potential of a factor 1.25 very close to the RLDM prediction for the major axis. We found that the level density of a nucleus of mass $A \sim 60$ at $J \sim 35\hbar$ and $E_x = 17$ MeV is roughly 2 orders of magnitude larger than that corresponding to a spherical shape. Level density enhancements have been evidenced in the past for statically deformed nuclei[7,8] and are predicted also for dynamically deformed nuclei.[37,38]

The statistical model used in this work is able to reproduce all the measured observables, including those representing specific subsets of decay paths such as the light-particle–light-particle correlations and the spectral shapes of relatively rare decay modes as $d$ and $t$ emission. Complete model calculations are an important technique to describe correctly and in detail the decay of an equilibrated compound nucleus and to determine properties of hot rotating nuclei.

## ACKNOWLEDGMENTS

We acknowledge the participation of A. Bracco, I. Iori, and A. Moroni at the first data taking of this work. We thank M. G. Mustafa for providing the calculated shape parameters. This work was supported by the Istituto Nazionale di Fisica Nucleare, the U.S. Department of Energy, and the Robert A. Welch Foundation. One of us, J.B.N., thanks the Laboratori Nazionali di Legnaro for the kind hospitality accorded during this experiment.

*Present address: Dipartimento di Fisica dell' Università di Bari, I-70126 Bari, Italy.

†Permanent address: Institute of Nuclear Physics, Cracow, Poland.

[1]E. Vogt, in *Advances in Nuclear Physics*, edited by M. Baranger and E. Vogt (Plenum, New York, 1968), Vol. 1, p. 261.

[2]R. G. Stokstad, in *Treatise on Heavy-Ion Science*, edited by D. A. Bromley (Plenum, New York, 1985), Vol. 3, p. 83.

[3]S. Bjornholm, A. Bohr, and B. R. Mottelson, *Proceedings of the Third International Symposium on the Physics and Chemistry of Fission, Rochester, 1973* (I.A.E.A., Vienna, 1974), Vol. 1, p. 367.

[4]M. Blann and T. T. Komoto, Phys. Rev. C **24**, 426 (1981).

[5]S. Cohen, F. Plasil, and W. Swiatecki, Ann. Phys. (N.Y.) **82**, 557 (1974).

[6]S. E. Vigdor and H. J. Karwowski, Phys. Rev. C **26**, 1068 (1982).

[7]J. R. Huizenga, A. N. Behkami, J. S. Sventek, and R. W. Atcher, Nucl. Phys. **A223**, 589 (1974).

[8]T. Dossing and A. S. Jensen, Nucl. Phys. **A222**, 493 (1974).

[9]M. Blann, Phys. Rev. C **21**, 1770 (1980).

[10]N. N. Ajitanand *et al.*, Nucl. Instrum. Methods **A243**, 111 (1986), and references therein.

[11]R. K. Choudhury *et al.*, Phys. Lett. **143B**, 74 (1984), and references therein.

[12]F. Puhlhofer *et al.*, Phys. Rev. C **16**, 1010 (1977).

[13]T. M. Cormier *et al.*, Phys. Rev. C **15**, 654 (1977).

[14]B. Fornal *et al.*, Phys. Rev. C **37**, 2624 (1988).

[15]G. Rosner *et al.*, Phys. Lett **150B**, 87 (1985).

[16]G. La Rana *et al.*, Phys. Rev. C **35**, 373 (1987).

[17]Z. Majka *et al.*, Phys. Rev. C **35**, 2125 (1987).

[18]F. Puhlhofer, Nucl. Phys. **A280**, 267 (1977).

[19]D. W. Lang, Nucl. Phys. **77**, 545 (1966).

[20]W. Dilg, W. Schantl, H. Vonach, and M. Uhl, Nucl. Phys. **A217**, 269 (1973).

[21]D. Wilmore and P. E. Hodgson, Nucl. Phys. **55**, 673 (1964); P. E. Hodgson, Annu. Rev. Nucl. Sci. **17**, 1 (1967).

[22]F. G. Perey, Phys. Rev. **131**, 745 (1963).

[23]J. R. Huizenga and G. Igo, Nucl. Phys. **29**, 462 (1961).
[24]W. D. Myers and W. J. Swiatecki, Nucl. Phys. **81**, 1 (1966).
[25]M. G. Mustafa, P. A. Baisden, and H. Chandra, Phys. Rev. C **25**, 2524 (1982).
[26]A. J. Sierk, code BARFIT, Los Alamos National Laboratory, Group T9 (1984).
[27]For a revised version of the code PACE, see A. Gavron, Phys. Rev. C **20**, 230 (1980).
[28]T. Ericson, Adv. Phys. **9**, 425 (1960).
[29]C. C. Lu, L. C. Vaz, and J. R. Huizenga, Nucl. Phys. **A197**, 321 (1972).
[30]F. Pulhofer, Lect. Notes Phys. **117**, 334 (1980), and references therein.
[31]F. Bush *et al.*, Z. Phys. A **290**, 167 (1979).
[32]Tai Kuang Hsi, T. Dossing, C. Gaarde, and J. S. Larsen, Nucl. Phys. **A316**, 189 (1979).
[33]J. M. Lohr and W. Haberly, Nucl. Phys. **A232**, 381 (1974).
[34]F. D. Becchetti and G. W. Greenlees, in *Polarization Phenomena in Nuclear Reactions,* edited by H. H. Barschall and W. Haberly (The University of Wisconsin Press, Wisconsin, 1971), p. 682.
[35]L. C. Vaz and J. M. Alexander, Z. Phys. A **318**, 231 (1984).
[36]J. M. Alexander, D. Guerreau, and L. C. Vaz, Z. Phys. A **305**, 313 (1982).
[37]J. Toke and W. J. Swiatecki, Nucl. Phys. **A372**, 141 (1981).
[38]M. Barranco *et al.*, private communication.
[39]A. Bohr and B. R. Mottelson, *Nuclear Structure* (Benjamin, Reading, 1975), Vol. II.
[40]M. Kicinska-Habior *et al.*, Phys. Rev. C **36**, 612 (1987).